analytical chemistry

pubs.acs.org/ac Article

A Semi-Quantitative Isothermal Diagnostic Assay Utilizing Competitive Amplification

Christopher P. Mancuso,[⊥] Zhi-Xiang Lu,[⊥] Jason Qian,[⊥] Sarah A. Boswell, and Michael Springer*

Cite This: *Anal. Chem.* 2021, 93, 9541−9548 Read Online

ACCESS | Metrics & More | Article Recommendations | Supporting Information

ABSTRACT: Quantitative diagnostics that are rapid, inexpensive, sensitive, robust, and field-deployable are needed to contain the spread of infectious diseases and inform treatment strategies. While current gold-standard techniques are highly sensitive and quantitative, they are slow and require expensive equipment. Conversely, current rapid field-deployable assays available provide essentially binary information about the presence of the target analyte, not a quantitative measure of concentration. Here, we report the development of a molecular diagnostic test [quantitative recombinase polymerase amplification (qRPA)] that utilizes competitive amplification during a recombinase polymerase amplification (RPA) assay to provide semi-quantitative information on a target nucleic acid. We demonstrate that qRPA can quantify DNA, RNA, and viral titers in HIV and COVID-19 patient samples and that it is more robust to environmental perturbations than traditional RPA. These features make qRPA potentially useful for at-home testing to monitor the progress of viral infections or other diseases.

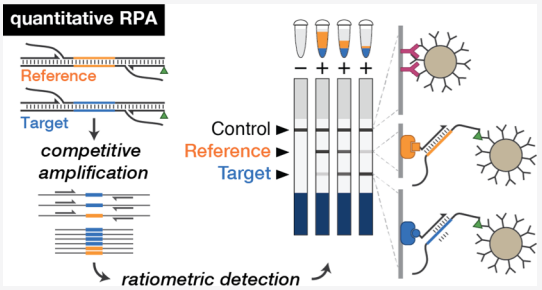

Downloaded via MARTIN LUTHER UNIV HALLE WITT on July 29, 2021 at 07:43:42 (UTC).
See https://pubs.acs.org/sharingguidelines for options on how to legitimately share published articles.

INTRODUCTION

Rapid, inexpensive, and sensitive testing is critical for controlling the spread of diseases with pandemic potential.[1] For example, as of 2019, one in five individuals with HIV do not know that they are infected,[2] and in many countries, efforts to contain SARS-CoV-2 have been hampered by a lack of adequate testing.[3] Rapid diagnostic testing with quantitative outputs can lead to more timely treatment and better knowledge of disease progression, leading to improved patient outcomes.[1] Nucleic acid amplification techniques (NAATs) are the gold standard for identifying infectious diseases.[4] To enable comprehensive diagnoses, NAATs need to provide specificity, sensitivity, and quantitation. Quantitative polymerase chain reaction (qPCR) is the most commonly used NAAT but requires expensive and complex instrumentation that cannot realistically be used outside the laboratory. For this reason, researchers have turned to isothermal nucleic acid amplification techniques (INAATs) in an attempt to create a field-deployable diagnostic.

Developing a field-deployable diagnostic is especially challenging if quantitative results are required. In many cases, a quality plus/minus result is sufficient, but in other cases, viral titer is a key factor in disease treatment. Current field-deployable INAATs are not quantitative. The products of INAATs [such as LAMP,[5] recombinase polymerase amplification (RPA),[6] HDA,[7] and NASBA][8] are generally interpreted in a non-specific manner by monitoring the amount of amplification (using DNA-intercalating or pH-sensitive dyes) or in a sequence-specific manner by detecting amplification products using lateral flow assays,[9] molecular beacons,[10] or Cas13-mediated fluorescence.[11] Because these reactions all proceed to saturation, the endpoint product levels do not depend on the input concentration. Furthermore, time course or "time-to-positive" measurements of these techniques are not robust due to the rapid speed of amplification and the sensitivity of the amplification rate to perturbations.[12] Finally, due to the lower reaction temperatures of many INAATs,[4] non-specific products are produced at higher rates than in qPCR, which affects sensitivity and further limits quantitation.

To overcome these challenges, we developed an assay that is both field-deployable and semi-quantitative by harnessing competitive amplification in an RPA assay. We selected RPA as the basis of our assay as it can be performed near ambient temperature (37−42 °C). In RPA, a cocktail of recombinase enzymes, single-stranded binding proteins, and DNA polymerases carry out cyclic strand invasion and polymerization to amplify DNA.[6] We previously developed an enhanced reverse transcription (eRPA) assay to detect SARS-CoV-2 RNA directly from patient samples with high sensitivity and specificity.[13] In this new assay, which we term quantitative recombinase polymerase amplification (qRPA), we introduce reference molecules that are competitively amplified alongside

Received: April 13, 2021
Accepted: June 16, 2021
Published: June 28, 2021

ACS Publications © 2021 American Chemical Society

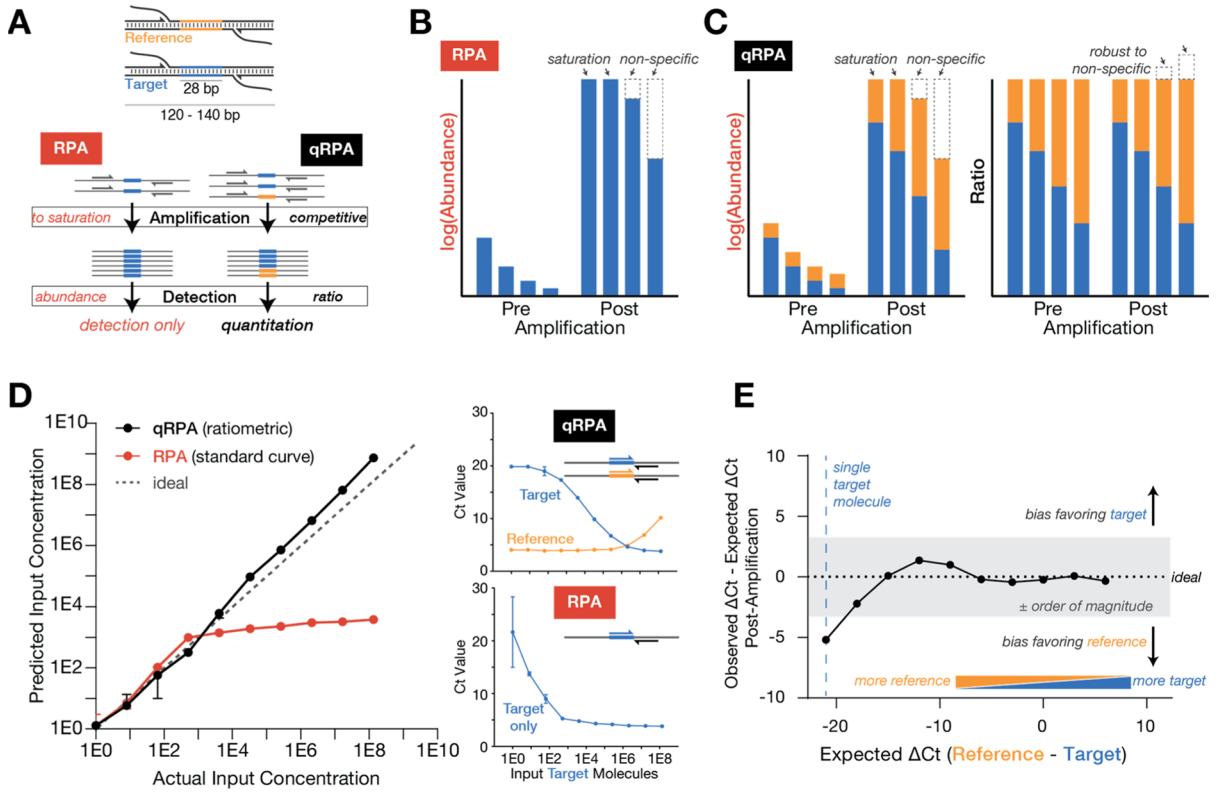

Figure 1. Competitive amplification in RPA can be used to maintain target concentration information. (A) In qRPA, addition of a reference molecule at a known concentration can be used to infer target concentration by measuring the ratio of the target to the reference after amplification. (B) RPA product levels saturate for high input concentrations and are affected by non-specific product formation, depicted by cartoon. (C) In qRPA, although product abundances are still subject to saturation and non-specific products, the ratio is robustly remained and can be used for quantification, depicted by cartoon. (D) Prediction of input concentration by endpoint measurements of RPA and qRPA. qPCR was used to quantify target or reference sequences after amplification by RPA or qRPA. The threshold cycle C_t values (right) were used to calculate a predicted input concentration either by fitting to a standard curve (RPA) or by calculating the target to reference ratio (qRPA). (E) Bland–Altman plot of qRPA outputs. The qRPA data were replotted to show the expected and observed ΔC_t, which indicates the target/reference ratio. Points are plotted against a horizontal line representing an ideal assay which retains ratiometric information perfectly. In each panel, each point depicts the mean of three replicate RPA or qRPA reactions, and error bars depict standard deviation.

the target (Figure 1A). Both amplicons are detected separately in a sequence-specific lateral flow assay for semi-quantitative endpoint detection. We demonstrate the efficacy of qRPA for DNA and RNA inputs as well as clinical samples from HIV and COVID-19 patients.

EXPERIMENTAL SECTION

RNA Template Generation. SARS-CoV-2 N-gene-containing plasmids were obtained from IDT (2019-nCoV Plasmid Controls). An HIV integrase gene containing plasmid was obtained from Jonathan Li's lab at Brigham and Women's Hospital. Genes were then cloned into a T7 promoter expression plasmid with or without reference sequence insertions using Gibson assembly. To produce the RNA template, in vitro transcription was performed with NxGen T7 RNA Polymerase (Lucigen) according to the manufacturer's suggested protocol with minor modifications. Final concentrations of the reaction mixture components were 50 units of T7 RNA polymerase, 1× reaction buffer, 625 μM nucleoside 5′-triphosphate, 10 mM dithiothreitol, 500 ng of the linearized plasmid template, and RNase-free water to a final volume of 20 μL per reaction. After 2 h at 37 °C, four units of DNase I (NEB) was added and reactions were further incubated for 10 min at 37 °C. DNase I was heat-inactivated by adding ethylenediaminetetraacetate (5 mM final) and heating at 75 °C for 10 min. RNA was purified using an RNAClean XP (Beckman Coulter) at 0.6× the volume of the reaction, washed twice with 80% EtOH, and then eluted into 20 μL of RNase-free water.

The concentration of each RNA stock was calculated based on a Poisson distribution of RT-qPCR measurements on dilution series of RNA in nuclease-free water down to 0.003 molecules/reaction.

qPCR Assays. Unless otherwise noted, SYBR green qPCR reactions were prepared in a 10 μL reaction volume using PowerUp SYBR Green PCR Master mix (Thermo Fisher Scientific), 2 μL of the sample, and 0.4 μM of primers and the following cycle conditions: (i) UDG activation: 50 °C for 2 min; (ii) denaturation: 95 °C for 2 min; (iii) amplification (45 cycles): 95 °C for 15 s, 60 °C for 60 s; (iv) melt curve: 95 °C to 60 °C. RT-qPCR reactions were prepared in a 10 μL reaction volume using the Luna Universal One-Step RT-qPCR kit (NEB), 2 μL of the sample, and 0.4 μM of primers and the following cycle conditions: (i) reverse transcription: 55 °C for 10 min; (ii) denaturation: 95 °C for 1 min; (iii) amplification (45 cycles): 95 °C for 10 s, 60 °C for 30 s; (iv) melt curve: 95–60 °C. TaqMan RT-qPCR reactions were prepared in a 10 μL reaction volume using the Luna Universal Probe One-Step RT-qPCR kit (NEB), 2 μL of the sample, 0.4 μM of primers, and 0.2 μM probe and the following cycle conditions: (i) UDG

https://doi.org/10.1021/acs.analchem.1c01576
Anal. Chem. 2021, 93, 9541−9548

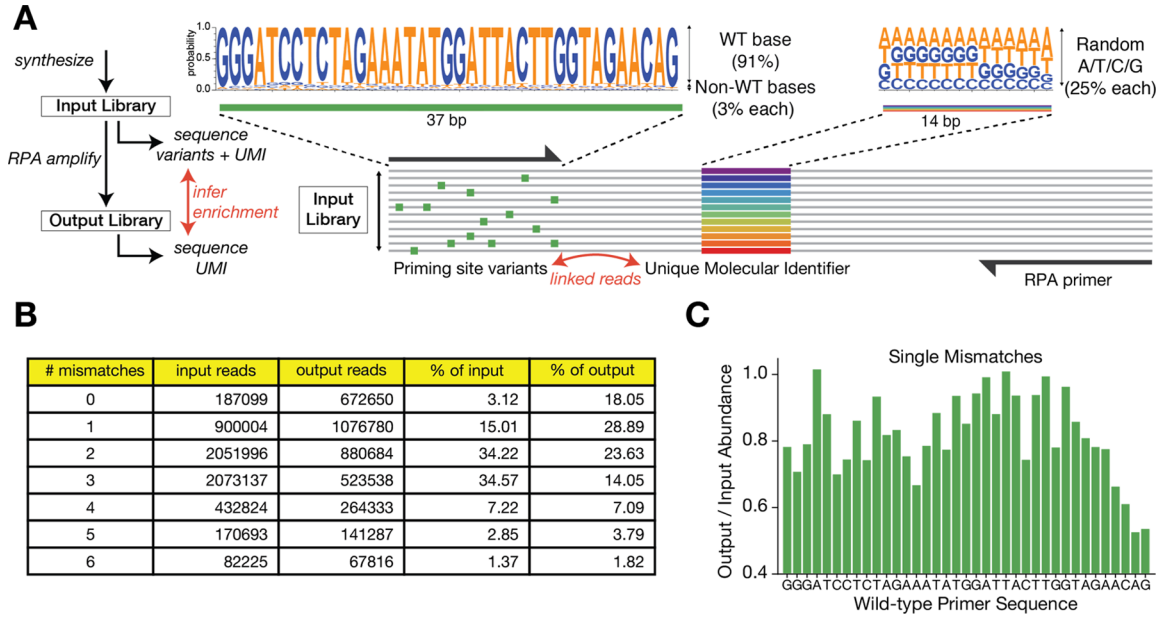

# mismatches	input reads	output reads	% of input	% of output
0	187099	672650	3.12	18.05
1	900004	1076780	15.01	28.89
2	2051996	880684	34.22	23.63
3	2073137	523538	34.57	14.05
4	432824	264333	7.22	7.09
5	170693	141287	2.85	3.79
6	82225	67816	1.37	1.82

Figure 2. qRPA is robust to certain sequence variations. (A) Measurement of amplification bias from sequence variation. A library with random sequence mismatches in the forward priming region with each linked to internal UMI sequences was synthesized. This input library was amplified using RPA, and then, both input and output libraries were sequenced. (B) Frequency table for reads in the input and output libraries, grouped by number of mismatches in priming sequence. (C) Abundance of library members with a single mismatch in the priming sequence, plotted by mismatch location, with output library abundance normalized by input library abundance.

activation: (i) reverse transcription: 55 °C for 10 min; (ii) denaturation: 95 °C for 1 min; (iii) amplification (45 cycles): 95 °C for 10 s, 55 °C for 30 s. All qPCR and RT-qPCR reactions were monitored on a QuantStudio 6 Real Time PCR system (Thermo Fisher Scientific) or CFX96 real-time PCR system (Bio-Rad). The primers and probes used in reactions can be found in Table S1, and the corresponding amplicons may be found in Table S2.

qRPA and RT-qRPA Assays. Unless otherwise noted, qPRA assays were based on the TwistAmp Basic RPA Kit (TwistDx) with added modifications described below. For qRPA, each lyophilized pellet was resuspended in a solution of 39.5 μL of the rehydration buffer (TwistDx) and 0.5 μL of the forward and reverse primer mixes each at 50 μM. For RT-qRPA, 1.5 μL of the rehydration buffer was replaced with 1 μL of RNase H (5 U/μL) (NEB) and 0.5 μL of SuperScript IV RT (200 U/μL) (Thermo Fisher Scientific). The qRPA or RT-qRPA mix was then activated by addition of 1 μL of 700 mM magnesium acetate, followed by thorough mixing with a pipette. Reactions were prepared by dispensing 7.5 μL of the master mix, 0.5 μL of the reference template, and 2 μL of the sample input per reaction well; mixing the reaction mixture by pipetting; and incubating at 42 °C for 25 or 30 min. Unless otherwise noted, a hybridization mix was prepared by combining 1 μL of the target-specific biotinylated probe at 5 μM (HIV JQ130; SARS-CoV-2 JQ241) and 1 μL of the reference digoxigenated probe (JQ170) with 18 μL of 10 mM Tris pH 8. 20 μL of the hybridization mix was added to each reaction, and samples were heated at 94 °C for 3 min, followed by a cooling step at room temperature for 3 min. 50 μL of Milenia GenLine 2T Buffer (Milenia Biotec) was added to each reaction and mixed by pipetting, and a lateral flow strip (Milenia HybriDetect 2T) was added. Lateral flow strip signals can be detected and imaged starting 3 min after addition of the strip to the hybridized reaction. Test results were called or imaged within 45 min of strip addition since background bands at the test and reference lines can appear over time and low signal test bands can lose intensity as the strip dries.

In the pH and salt perturbation qRPA assay, homemade 2× rehydration buffer was prepared to contain 50 mM Tris, 200 mM potassium acetate, and 11% (w/v) polyethylene glycol (PEG) 20,000. For pH perturbations, buffer pH was adjusted by hydrochloric acid or sodium hydroxide and measured using a pH meter. For salt perturbations, NaCl was added to 120 mM. Each lyophilized pellet (TwistDx) was resuspended by a homemade rehydration buffer to form 50 μL of final 1× solution with 25 mM Tris, 100 mM potassium acetate, 5.5% (w/v) PEG 20,000, 700 mM magnesium acetate, and 240 nM primers.

Sequencing Analysis of the Primer Mutational Library. A mutational template library (JQ75) where each base pair constitution of the forward RPA primer binding site (JQ42) was 91% as the wild-type base and 3% of each of the three remaining bases was ordered from Integrated DNA Technologies. Additionally, another library (JQ76) with 14-bp randomized Unique Molecular Identifier (UMI) was designed 11-bp downstream of the forward RPA primer binding site to associate UMI to template variants (Figure 2A). Template variant and UMI libraries were PCR-amplified with sequencing adaptors (JQ77,83-85 and JQ93-96) and then indexing primers (Table S3) to build the input library. The input library was used as an input template into a 50 μL RPA reaction, where a lyophilized pellet was resuspended in a solution of 29.5 μL of the rehydration buffer (TwistDx) and 480 nM of the forward primer (JQ42) and reverse primer (JQ92) and 1 μL of the input library and supplemented with RNAse-free water until 47.5 μL, which was then activated by addition of 2.5 μL of 280 mM magnesium acetate, followed by thorough mixing with a pipette. The post-RPA amplification product was purified with 0.8× AMPure XP beads (Beckman Coulter) and was PCR-amplified with sequencing adaptors (JQ97-100 and JQ93-96) and then indexing primers (Table

https://doi.org/10.1021/acs.analchem.1c01576
Anal. Chem. 2021, 93, 9541−9548

S3) to build the output library. The input and output libraries were sent for sequencing (paired-end 150-bp) on NextSeq550 (Illumina). For the bioinformatics analysis, Paired-End reAd mergeR was used to merge read 1 and read 2 of both input and output sequenced libraries. Seqtk was then used to filter out reads smaller than 50-bp in length. Then, from the input library sequencing reads, a look-up table of primer variants of 37-bp matched to 14-bp UMIs was built. Individual barcodes that were matched to multiple different primer variants were discarded. Output library 14-bp UMIs were extracted from output sequencing reads and matched to primer variants based on the look-up table.

Clinical HIV Samples. A cohort of RNA extract samples were obtained from Jonathan Li's lab at Brigham and Women's Hospital, collected from patients with an estimated HIV viral load of 15,000 or 1500 copies/mL. Replicate 200 mL plasma samples were extracted using a Norgen Biotech Kit and eluted into 55 μL of the buffer according to the manufacturer's instructions and then stored at −80 °C. At the time of testing, replicate samples were pooled in groups of three and vacuum-concentrated to 15−20 μL (such that sample inputs were ∼30× more concentrated than plasma). 2 μL of the concentrated sample was used as input into RT-qRPA or RT-qPCR reactions.

Clinical COVID Samples. A cohort of nasal swab patient samples was purchased from BocaBiolistics, FL. Samples were thawed on ice, and 40 μL aliquots were made and subsequently stored at −80 °C. At the time of testing, sample aliquots were thawed and RNasin Plus was added to a final concentration of 1 U/μL. The samples were placed on a heat block set to 99 °C for 5 min for virus inactivation and lysis. After cooling, samples were spun down and transferred to a 96-well DNA LoBind plate (Eppendorf). 2 μL of the inactivated sample was used as input into RT-qRPA or RT-qPCR reactions.

Quantitative Image Analysis of Lateral Flow Assays. Lateral flow assays per sample were photographed under ambient lighting using a smartphone camera. The pixel intensity was measured using ImageJ for an equivalent area of each lateral flow strip. Intensities were normalized to correct for uneven lighting such that normalized intensity $I_{norm} = 1 - (I - I_{control})/(\text{median}(I) - I_{control})$, where $I_{control}$ represents the darkest point of the control band. Any sample for which $I_{target,norm} > 0.02$ or $I_{target,norm} > I_{reference,norm}$ was classified as positive for calculating sensitivity and specificity. Linear regression was used to correlate the ratio of $I_{target,norm}/I_{reference,norm}$ to the target concentration for all positive samples. If multiple assays were performed at different reference ratios, linear regression was performed on the mean of the $I_{target,norm}/I_{reference,norm}$ ratios instead in order to predict the sample titer.

RESULTS AND DISCUSSION

Competitive Amplification in RPA Can Be Used to Maintain Target Concentration Information. As noted above, endpoint INAATs are not quantitative for two reasons. First, in RPA, amplification continues until reaction components are exhausted, leading to signal saturation. Saturation is reached regardless of the amount of input material, and thus, input concentration information is largely lost (Figure 1B). Second, INAATs are prone to non-specific product formation.[4] The specific amplification is dependent on the target level, but the non-specific amplification is dependent on primer levels and non-specific template formation. Thus, when the input level of the target is low, non-specific side reactions can outcompete the on-target reaction, consuming significant amounts of the reaction components and reducing the amount of target amplicon produced (Figure 1B). We reasoned that RPA could be made quantitative by harnessing competition during amplification. Non-specific side reactions cause a decrease in endpoint target amplicon levels so that the correlation between target input levels and amplicon level is modest at assay completion (Figure 1B). Rather than relying on stochastic and uncontrolled side reactions, we include a reference molecule in the RPA assay; we refer to this modified RPA reaction as qRPA. In theory, the ratio of the target and reference sequence should stay constant throughout the RPA reaction as long as both the target and reference sequence have the same amplification kinetics (Figure 1C). The easiest way to achieve this is to have both the target and reference molecules amplified by the same RPA primer set (Figure 1A).

To compare the performance of RPA and qRPA, we performed both reactions on varying amounts of plasmid DNA containing a synthetic 28-bp barcode target.[14] For the qRPA reaction, we also included a fixed concentration of a reference plasmid that was identical except in the synthetic barcode sequence. We quantified the products by qPCR using a barcode-specific primer paired with one universal primer (in a separate qPCR reaction for each barcode) (Figure 1D, right). In RPA, as the target input reaches single-molecule levels, there is great variation in the amount of amplification, likely due to the stochastic difference in timing of the initial production of non-specific products (Figure 1D, right). Amplification appears to be less variable in the qRPA reactions.

We assessed the quantitative capabilities of RPA and qRPA by using endpoint measurements as predictors of the input concentration. We calculated a predicted input concentration for each assay using the cycle threshold values (C_t), which we either fit to a standard curve (RPA) or calculate using the target to reference ratio (qRPA) (Figure 1D, left). While the RPA assay saturates at high input concentrations, qRPA remains quantitative over a wide range of target input concentrations. In a Bland−Altman plot, if the assay maintains the ratio perfectly, the difference between the observed and expected ΔC_t (the cycle threshold of the reference minus the cycle threshold of the target) would be a horizontal line. Indeed, we find that the ratio between the target and reference is maintained during amplification for a wide range (>10^7-fold difference) of starting target/reference ratios (Figure 1E). This confirms that input concentration may be inferred from the known amount of reference added and the ratio between target and reference molecules after amplification.

qRPA is Robust to Environmental Perturbations and Sequence Variations. We hypothesized that qRPA should be more robust to environmental perturbation than RPA since if the amplification kinetics of the target and reference sequences are identical, the ratio of the target and reference amplicons should be maintained regardless of reaction efficiency. To test this prediction, we performed RPA under several environmental perturbations that might be faced in real-world settings, including different temperatures, pH, and salt concentrations. We quantified the post-amplification products by qPCR as described above. For reactions at pH 2.4 or pH 11.4 or with 60 mM additional NaCl, the amount of amplification product produced was less predictive of the input level than under standard conditions (Figure S1); since these effects are mild, we can infer that RPA efficiency is little affected by these conditions. Nevertheless, the ratiometric

https://doi.org/10.1021/acs.analchem.1c01576
Anal. Chem. 2021, 93, 9541−9548

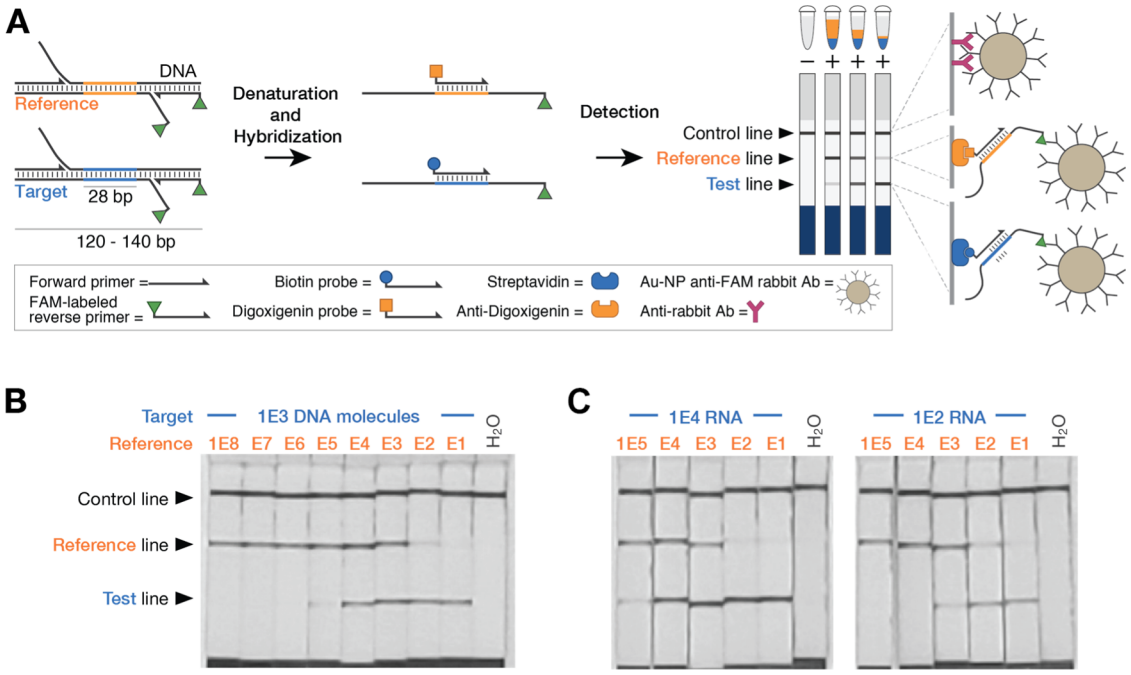

Figure 3. qRPA can be combined with a lateral flow assay for fieldable detection. (A) Target and reference amplicons are detected using different hybridization probes and visualized using gold nanoparticles on lateral flow strips in a multiplexed sandwich assay. The relative intensity of target and reference bands can be used to infer target concentration in the sample. (B) Samples were prepared with 1E3 copies of a plasmid carrying a wild-type SARS-CoV-2 N-gene sequence and a varying number of copies of a reference plasmid in which a 28-bp region of the target was replaced with a synthetic barcode. These samples were amplified using qRPA, hybridized with target and reference probes, and visualized on the photographed lateral flow strips. Bands of equal intensity are observed when the target and reference concentrations are equal. (C) RNA was prepared from these plasmids using in vitro transcription, quantified using RT-qRPA, and visualized as above.

product levels are robust to all three variant conditions, so qRPA remains quantitative even when amplification efficiencies are affected by environmental perturbations (Figure S1). RPA can be performed at different temperatures,[15] but lower temperatures are known to reduce amplification speed. We found qRPA to be robust to temperature variation and reaction time even when the target C_t levels are reduced by sub-optimal temperatures or sub-saturating reaction lengths which would cause an underestimate if fitting RPA product levels to a standard curve (Figure S2).

Detection of disease can also be hampered by sequence variation that arises during disease spread. This sequence variation can interfere with amplification reactions, particularly if the variation occurs in the 3′ end of the priming region. Since the qRPA method relies on the reaction kinetics for target and reference molecules being equal, quantitation might be affected if the priming efficiencies are affected by mutations. RPA primer efficiencies are known to significantly affect the degree of amplification,[6,16] and polymorphisms in priming regions have been shown to affect the sensitivity of other isothermal amplification diagnostics.[17] To quantify the potential impact of sequence variation on qRPA, we sequenced a library of RPA primer-region variants before and after amplification with RPA (Figure 2A). The library was created by degenerate synthesis of a 37-bp RPA primer-region sequence with 91% abundance of the original nucleotide and 3% abundance of the other three nucleotides in the RPA primer binding region. This leads to an average error rate of 3.3 mismatches per template (Figure S3). In addition, each template had a random 14bp UMI in the region that would be amplified. Thus, by comparing the UMI sequence before and after amplification, it is possible to determine which mutations in the forward RPA primer-region affect RPA amplification (Figure 2A). Amplification bias was largely confined to the 3′ end of the RPA primer sequence (Figure 2C), suggesting that qRPA is robust to the majority of mutations that may occur in the primer-region sequence, even if multiple polymorphisms co-occur (Figure 2B). This result also has implications for the optimal design of RPA primers, suggesting that primers with 3′ ends aligning to highly conserved regions in the target may be more robust to inevitable mutational variation.

Combining qRPA with a Lateral Flow Assay for Fieldable Detection. qRPA can be combined with a fieldable detection method to measure the ratio of target and reference amplicons and then to infer the input concentration. We followed qRPA with hybridization with two probes, one biotinylated and complementary to the target sequence and one digoxigenin labeled and complementary to the reference sequence. This mixture was heat-denatured, allowed to cool, and then run on a lateral flow strip to quantify the relative abundance of target and reference amplicons in the reaction (Figure 3A). We chose to use Milenia Biotec HybriDetect 2T lateral flow test strips that contain a streptavidin band, an anti-digoxigenin band, and an anti-Ig band. These complexes are visualized using gold nanoparticle-labeled anti-FAM antibodies that are captured at either test or reference bands on the lateral flow assay strip. To demonstrate this method, we cloned the N-gene of SARS-CoV-2 into a plasmid and generated a reference target plasmid in which we replaced the RPA target portion of the sequence with a 28-bp reference barcode. We performed qRPA on a mixture of wild-type and barcoded-reference plasmids to demonstrate quantitation on lateral flow assays. The relative intensity of the reference and target bands for one or more reference concentrations can be used to infer

https://doi.org/10.1021/acs.analchem.1c01576
Anal. Chem. 2021, 93, 9541−9548

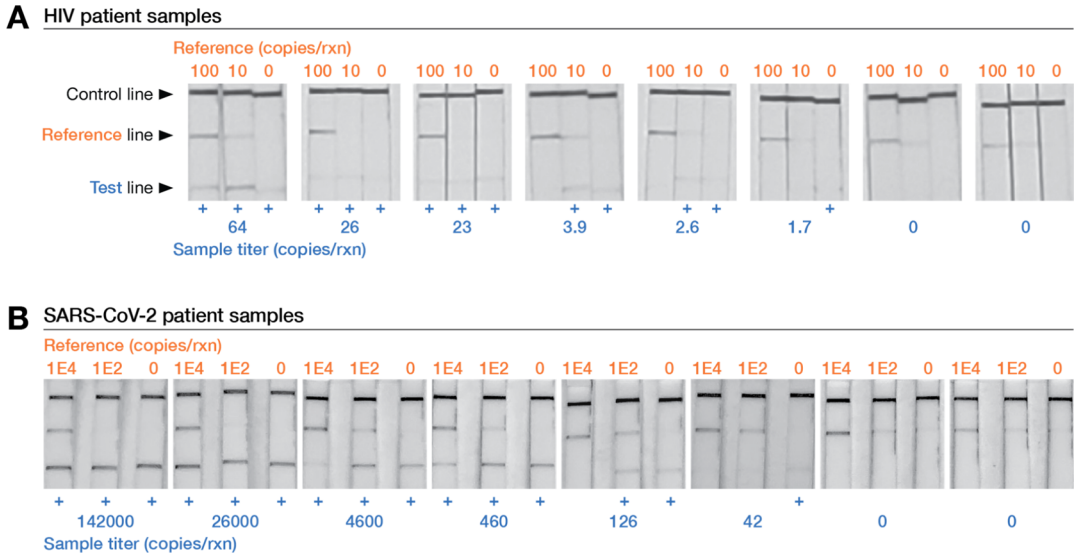

Figure 4. RT-qRPA and lateral flow assays can be used to quantify viral titers in patient samples. (A) Total RNA was extracted from whole blood samples from HIV (+) or (−) patients. Known quantities of in vitro HIV reference RNA containing a synthetic barcode were added to patient samples and amplified in qRPA. The photograph depicts a selection of lateral flow strips used to sort patient samples by viral titer. (B) Remnant nasopharyngeal swab samples from SARS-CoV-2 (+) or (−) patients were tested without extraction. Known quantities of in vitro SARS-CoV-2 reference RNA containing a synthetic barcode were added to patient samples and amplified in qRPA. The photograph depicts a selection of lateral flow strips used to sort patient samples by viral titer.

the concentration of a target DNA input with roughly 1 order of magnitude precision (Figure 3B).

Developing a One-Step RT-qRPA Assay to Quantify RNA. Many pathogens are composed of RNA genomes, including widespread pathogens such as HIV and SARS-CoV-2. qRPA may be combined with reverse transcription in a one-step RT-qRPA assay for RNA quantitation. We hypothesized that as long as the reverse transcriptase reaction does not exhibit significant bias, the ratio of RT-RPA products should be retained in an RT-qRPA assay. Building on our previously reported eRPA assay for one-pot RNA amplification,[13] we tested whether RT-qRPA could be used to quantify RNA input levels. We cloned the integrase gene from HIV into a plasmid and replaced the RPA target portion of the sequence with our 28-bp reference barcode (to be used as the reference sequence). We generated RNA from wild-type and barcoded-reference plasmids using in vitro transcription (IVT) and then performed qRPA using combinations of these RNA products. Comparing the input ratio of target and reference RNA (pre-amplification) by RT-qPCR and post-amplification by qPCR, we found that RT-qRPA retains the product ratio over several orders of magnitude (Figure S4) with comparable performance to TaqMan RT-qPCR (Figure S5). The amplicons can be detected using lateral flow analysis in a field-deployable manner as had been shown with DNA targets (Figures 3C and S6). We obtained comparable results to the HIV constructs with RNA produced from the wild-type and barcoded-reference SARS-CoV-2 N-gene plasmids described above (Figures S4 and S6). Finally, by comparing the results from using several different reference molecule types (e.g., RNA, cDNA, and DNA), we determined that for detection of RNA targets, an RNA reference molecule is most appropriate (Figure S7).

Using RT-qRPA and Lateral Flow Assays to Quantify Viral Titers in Patient Samples. To validate our assay for diagnostic use in quantifying viral load in the context of clinical samples, we developed a qRPA assay for HIV. HIV patients on anti-retroviral therapies may have varying viral loads that vary over time with treatment efficacy;[18] viral load also correlates with transmissibility,[19] so inexpensive rapid testing could enable better risk assessment. Viral loads <1500/mL are often considered to be non-transmissible.[19] We performed qRPA on RNA samples extracted from the blood of individuals that were positive or negative for HIV. Using a trio of qRPA reference standards (0, 10, or 100 copies of reference RNA, corresponding to viral loads of no, 1500/mL, or 15000/mL in unextracted blood), we classified 13 HIV patient and healthy samples (Figures 4A and S8). To test the assay over a higher range of viral loads, we created and tested contrived positive samples by spiking our HIV IVT RNA into RNA samples purified from HIV-negative blood samples (Figure S8). We subsequently asked three different individuals to estimate the titer of blinded samples, and 85% of these calls were within an order of magnitude of the true titer (Table S1), with a sensitivity of 92% and a specificity of 79%. Bland−Altman plots show that the pre- and post-qRPA amplification ratios as measured by qPCR were generally conserved (Figure S9), as expected from our in vitro validation experiments.

Finally, we demonstrated that qRPA can also be used to quantitate SARS-CoV-2 levels in unextracted clinical samples. Blood interferes with many molecular assays and hence some form of extraction is needed, whereas nasal swabs are directly compatible with molecular assays.[13] We therefore wanted to test the ability of qRPA to quantify SARS-CoV-2 titer directly from nasal swabs. We ran qRPA on remnant nasopharyngeal swab samples suspended in the transport medium from individuals that were positive or negative for COVID-19. Using a trio of qRPA reference standards (0, 100, or 10,000 copies of reference RNA), we classified 22 patient samples by viral loads with order-of-magnitude precision (with one false negative on the sample with the lowest viral load) and confirmed 36 negative patient samples (Figures 4B and S10). We subsequently asked three different individuals to estimate the titer of blinded samples, and 95% of these calls were within

https://doi.org/10.1021/acs.analchem.1c01576
Anal. Chem. 2021, 93, 9541−9548

an order of magnitude of the true titer (Table S2). Across all 58 samples tested, the overall sensitivity of 95% and a specificity of 97% were found. Post-amplification ratios were biased in favor of the unencapsulated reference over the virus-encapsulated target, which may indicate that RPA is less efficient at releasing and amplifying viral RNA than qPCR (Figure S9). This bias could be overcome by adjusting the amount of reference loaded or by developing viral mimics for use as reference species (e.g., AccuPlex[20]).

To provide more detailed quantitation from qRPA lateral flow assays, we analyzed assay images to infer target concentration from the ratio of band intensities. We used ImageJ to analyze photographs of the HIV and COVID-19 lateral flow assays that had been scored by our blinded individuals. After normalizing by the control band intensity and the median intensity of the strip (to control for uneven illumination and different camera settings), we calculated the intensity of the test band and reference band for the trio of strips from each sample. As expected, we observed a correlation between the input target concentration and the ratio of intensities for the test and reference bands. Using the mean intensity ratio across the trio of strips for each sample, we predicted the titer of our positive patient samples for HIV (R^2 = 0.90) and COVID-19 (R^2 = 0.76); predicted titers were within 1 order of magnitude of the true titer for 100% of HIV-positive samples and 89% of SARS-CoV-2-positive samples (Figure S11). More accurate classifications may be achieved with controlled lighting conditions or more sophisticated analysis software.[21,22]

DISCUSSION

qRPA uses competitive amplification and multiplexed detection to create an assay that could be used in field-deployable settings that require quantitation. Competitive amplification of the target and reference amplicons overcomes the challenges posed by non-specific amplification for quantitation, and lateral flow detection provides a simple read-out. The method works with both purified DNA and RNA as well as unextracted nasal swab samples.

qRPA overcomes many of the limitations of other isothermal amplification and detection techniques with semi-quantitative outputs. Competitive-LAMP also utilizes competitive amplification to enable order-of-magnitude quantitation of nucleic acids with similar sensitivity and specificity,[23] but qRPA benefits from simpler assay design (fewer primers) and lower reaction temperatures (LAMP is performed at 65 °C). In addition, multiplexed detection of target and reference molecules on the lateral flow strip provides more data per reaction, so fewer reactions are needed to determine concentration in qRPA than competitive-LAMP. Real-time RPA utilizing exo probes (and enzymatic hydrolysis) can also be used for time-to-positive dynamic measurements for direct quantitation[6] or ratiometric quantitation.[12] However, this approach requires sensitive real-time fluorescence measurements and internally modified probes that are difficult to manufacture at scale. Finally, although direct sample quantitation without amplification may soon be possible for highly concentrated nucleic acid targets,[24] qRPA (and other amplification techniques) can achieve higher sensitivities while remaining semi-quantitative.

Further work should broaden the use of qRPA to additional settings, sample types, and detection methods. First, there is a need for INAATs that can be run at ambient temperatures for point-of-need, equipment-free testing. RPA and qRPA can be performed at ambient temperatures but at reduced speeds; it may be possible to overcome this by optimizing reaction mixes for ambient temperature reaction rates. Second, some sample types will likely remain challenging for RPA. One notable example, unextracted blood samples, could be made compatible with qRPA by using low-cost nucleic acid extraction methods.[25] More broadly, validation of ratiometric amplification by post-amplification qPCR will be required in the development stage for each new sample type. Finally, on the detection side, we believe that the competitive amplification methods used in this work combined with multiplexed fluorescence detection using SHERLOCK[11,26] or molecular beacon[10] approaches could overcome challenges in using these detection methods for endpoint samples.

We believe that qRPA is well suited for non-laboratory settings where quantitation is needed for diagnosis. Measuring relative viral load in equipment-limited settings could help combat the AIDS pandemic by tracking the efficacy of antiretroviral therapies.[18] qRPA also brings us closer to at-home testing to track the progress of viral infections like SARS-CoV-2 following a positive test, which could help determine transmission risk and ease the load on laboratory testing facilities.[27] More broadly, higher-throughput, lower-precision testing for infectious diseases outside laboratories enabled by isothermal techniques will have value for contact tracing and epidemiological purposes[1] and pandemic control.

ASSOCIATED CONTENT

Supporting Information

The Supporting Information is available free of charge at https://pubs.acs.org/doi/10.1021/acs.analchem.1c01576.

Primer design; qRPA performed with chemical, temperature, and time perturbations; Bland–Altman plots of qRPA and RT-qRPA; photographs of all lateral flow assays; quantitative image analysis predictions of sample titers; blinded classification results; and list of primers, probes, and amplicons (PDF)

AUTHOR INFORMATION

Corresponding Author

Michael Springer − *Department of Systems Biology, Harvard Medical School, Boston, Massachusetts 02115, United States; Laboratory of Systems Pharmacology, Harvard Medical School, Boston, Massachusetts 02115, United States; Massachusetts Consortium on Pathogen Readiness, Boston, Massachusetts 20115, United States*;
Email: michael_springer@hms.harvard.edu

Authors

Christopher P. Mancuso − *Department of Systems Biology, Harvard Medical School, Boston, Massachusetts 02115, United States*; orcid.org/0000-0002-3974-3480

Zhi-Xiang Lu − *Department of Systems Biology, Harvard Medical School, Boston, Massachusetts 02115, United States; Laboratory of Systems Pharmacology, Harvard Medical School, Boston, Massachusetts 02115, United States*

Jason Qian − *Department of Systems Biology, Harvard Medical School, Boston, Massachusetts 02115, United States; Laboratory of Systems Pharmacology and Biological and Biomedical Sciences Program, Harvard Medical School,*

https://doi.org/10.1021/acs.analchem.1c01576
Anal. Chem. 2021, 93, 9541−9548

Boston, Massachusetts 02115, United States; orcid.org/0000-0002-1144-2547

Sarah A. Boswell − *Department of Systems Biology, Harvard Medical School, Boston, Massachusetts 02115, United States; Laboratory of Systems Pharmacology, Harvard Medical School, Boston, Massachusetts 02115, United States;* orcid.org/0000-0002-3118-3378

Complete contact information is available at: https://pubs.acs.org/10.1021/acs.analchem.1c01576

Author Contributions

⊥C.P.M., Z.-X.L., and J.Q. contributed equally to this work.

Author Contributions

Z.-X.L., J.Q., S.A.B, and M. S. conceived the study. C.P.M., Z.-X.L., J.Q., and S.A.B. performed the key experiments. J.Q. performed the sequencing analysis. All authors wrote the paper.

Notes

The authors declare the following competing financial interest(s): M.S. is inventor on U.S. Provisional Patent Application 63/003,555 (Harvard Case #8153). All other authors declare no competing interests.

■ ACKNOWLEDGMENTS

We would like to thank Autumn Kittilson and Jonathan Li from Brigham and Women's Hospital for HIV sample collection and extraction. We would also like to thank other members of the Springer lab and the members of the Khalil lab at Boston University for thoughtful discussions. This work was supported by DARPA BRICS HR0011-18-2-0014, the Quadrangle Fund for the Advancement and Seeding of Translational Research at Harvard Medical School (Q-FASTR), and the China Evergrande Group. J.Q. is supported by NSF GRFP. M.S. is supported by R01 GM120122-01.

■ REFERENCES

(1) Caliendo, A. M.; Gilbert, D. N.; Ginocchio, C. C.; Hanson, K. E.; May, L.; Quinn, T. C.; Tenover, F. C.; Alland, D.; Blaschke, A. J.; Bonomo, R. A.; Carroll, K. C.; Ferraro, M. J.; Hirschhorn, L. R.; Joseph, W. P.; Karchmer, T.; MacIntyre, A. T.; Reller, L. B.; Jackson, A. F.; Infectious Diseases Society of America (IDSA). *Clin. Infect. Dis.* **2013**, *57*, S139.

(2) Joint United Nations Programme on HIV/AIDS. *Global AIDS Update 2019—Communities at the Centre*, 2019.

(3) Cheng, M. P.; Papenburg, J.; Desjardins, M.; Kanjilal, S.; Quach, C.; Libman, M.; Dittrich, S.; Yansouni, C. P. *Ann. Intern. Med.* **2020**, *172*, 726−734.

(4) Obande, G. A.; Banga Singh, K. K. *Infect. Drug Resist.* **2020**, *13*, 455−483.

(5) Notomi, T.; Okayama, H.; Masubuchi, H.; Yonekawa, T.; Watanabe, K.; Amino, N.; Hase, T. *Nucleic Acids Res.* **2000**, *28*, No. e63.

(6) Piepenburg, O.; Williams, C. H.; Stemple, D. L.; Armes, N. A. *PLoS Biol.* **2006**, *4*, No. e204.

(7) Vincent, M.; Xu, Y.; Kong, H. *EMBO Rep.* **2004**, *5*, 795−800.

(8) Compton, J. *Nature* **1991**, *350*, 91−92.

(9) Koczula, K. M.; Gallotta, A. *Essays Biochem.* **2016**, *60*, 111−120.

(10) Tyagi, S.; Bratu, D. P.; Kramer, F. R. *Nat. Biotechnol.* **1998**, *16*, 49−53.

(11) Gootenberg, J. S.; Abudayyeh, O. O.; Kellner, M. J.; Joung, J.; Collins, J. J.; Zhang, F. *Science* **2018**, *360*, 439−444.

(12) Crannell, Z. A.; Rohrman, B.; Richards-Kortum, R. *Anal. Chem.* **2014**, *86*, 5615−5619.

(13) Qian, J.; Boswell, S. A.; Chidley, C.; Lu, Z.-x.; Pettit, M. E.; Gaudio, B. L.; Fajnzylber, J. M.; Ingram, R. T.; Ward, R. H.; Li, J. Z.; Springer, M. *Nat. Commun.* **2020**, *11*, 5920.

(14) Qian, J.; Lu, Z.-x.; Mancuso, C. P.; Jhuang, H.-Y.; del Carmen Barajas-Ornelas, R.; Boswell, S. A.; Ramírez-Guadiana, F. H.; Jones, V.; Sonti, A.; Sedlack, K.; Artzi, L.; Jung, G.; Arammash, M.; Pettit, M. E.; Melfi, M.; Lyon, L.; Owen, S. V.; Baym, M.; Khalil, A. S.; Silver, P. A.; Rudner, D. Z.; Springer, M. *Science* **2020**, *368*, 1135−1140.

(15) Lillis, L.; Lehman, D.; Singhal, M. C.; Cantera, J.; Singleton, J.; Labarre, P.; Toyama, A.; Piepenburg, O.; Parker, M.; Wood, R.; Overbaugh, J.; Boyle, D. S. *PLoS One* **2014**, *9*, No. e108189.

(16) Daher, R. K.; Stewart, G.; Boissinot, M.; Boudreau, D. K.; Bergeron, M. G. *Mol. Cell. Probes* **2015**, *29*, 116−121.

(17) Washington, N. L.; White, S.; Schiabor, K. M.; Cirulli, E. T.; Bolze, A.; Lu, J. T.; Washington, N. S Gene Dropout Patterns in SARS-CoV-2 Tests Suggest Spread of the H69del/V70del Mutation in the US. **2020**, medRxiv:20248814.

(18) Peter, T.; Ellenberger, D.; Kim, A. A.; Boeras, D.; Messele, T.; Roberts, T.; Stevens, W.; Jani, I.; Abimiku, A. l.; Ford, N.; Katz, Z.; Nkengasong, J. N. *Lancet Infect. Dis.* **2017**, *17*, e26−e29.

(19) Marks, G.; Gardner, L. I.; Rose, C. E.; Zinski, A.; Moore, R. D.; Holman, S.; Rodriguez, A. E.; Sullivan, M.; Giordano, T. P. *AIDS* **2015**, *29*, 947−954.

(20) Plachot, C.; Huang, C.; Vemula, R.; Wu, J.; Lee, H. J.; Anekella, B. *J. Clin. Virol.* **2016**, *82*, S49.

(21) Foysal, K. H.; Seo, S. E.; Kim, M. J.; Kwon, O. S.; Chong, J. W. *Sensors* **2019**, *19*, 4812.

(22) Urusov, A. E.; Zherdev, A. V.; Dzantiev, B. B. *Biosensors* **2019**, *9*, 89.

(23) Jiang, Y. S.; Stacy, A.; Whiteley, M.; Ellington, A. D.; Bhadra, S. *ChemBioChem* **2017**, *18*, 1692−1695.

(24) Fozouni, P.; Son, S.; Díaz de León Derby, M.; Knott, G. J.; Gray, C. N.; D'Ambrosio, M. V.; Zhao, C.; Switz, N. A.; Kumar, G. R.; Stephens, S. I.; Boehm, D.; Tsou, C.-L.; Shu, J.; Bhuiya, A.; Armstrong, M.; Harris, A. R.; Chen, P.-Y.; Osterloh, J. M.; Meyer-Franke, A.; Joehnk, B.; Walcott, K.; Sil, A.; Langelier, C.; Pollard, K. S.; Crawford, E. D.; Puschnik, A. S.; Phelps, M.; Kistler, A.; DeRisi, J. L.; Doudna, J. A.; Fletcher, D. A.; Ott, M. *Cell* **2021**, *184*, 323−333.

(25) Kolluri, N.; Albarran, N.; Fan, A.; Olson, A.; Sagar, M.; Young, A.; Gomez-Marquez, J.; Klapperich, C. M. *Lab Chip* **2020**, *20*, 3386−3398.

(26) Myhrvold, C.; Freije, C. A.; Gootenberg, J. S.; Abudayyeh, O. O.; Metsky, H. C.; Durbin, A. F.; Kellner, M. J.; Tan, A. L.; Paul, L. M.; Parham, L. A.; Garcia, K. F.; Barnes, K. G.; Chak, B.; Mondini, A.; Nogueira, M. L.; Isern, S.; Michael, S. F.; Lorenzana, I.; Yozwiak, N. L.; MacInnis, B. L.; Bosch, I.; Gehrke, L.; Zhang, F.; Sabeti, P. C. *Science* **2018**, *360*, 444−448.

(27) Esbin, M. N.; Whitney, O. N.; Chong, S.; Maurer, A.; Darzacq, X.; Tjian, R. *RNA* **2020**, *26*, 771−783.